IEEE CONTROL SYSTEMS LETTERS, VOL. 9, 2025

Distributed Resource Allocation for Human-Autonomy Teaming With Human Preference Uncertainty

Yichen Yao, *Student Member, IEEE*, Ryan Mbagna Nanko, Yue Wang, *Senior Member, IEEE*, and Xuan Wang, *Member, IEEE*

(Special Section on Safety, Robustness, and Effectiveness in Human–Machine Teaming)

***Abstract*— This letter investigates distributed resource allocation involving multiple autonomous agents and multiple humans, focusing on two challenges: (i) the dependency between autonomous and human agents through interaction; (ii) accounting for human uncertainties where both parties must collectively satisfy globally coupled probabilistic resource constraints. To address these, we first quantify the distribution of human choice behaviors using the maximum likelihood estimation (MLE), where human decisions evolve in response to nearby agent behaviors. Building on this human model, we introduce a novel reformulation that approximates the original probabilistic constraint via a polyhedral inner approximation, which then enables a fully distributed algorithm design over the system's communication graph while ensuring probabilistic constraint satisfaction. The proposed approach is validated through theoretical analysis and human-subject experiments.**

***Index Terms*—Distributed resource allocation, human-autonomy teaming, human preference uncertainty.**

I. Introduction

RESOURCE allocation is a fundamental problem in engineering systems [1], where heterogeneous agents must coordinate to share globally coupled resources while optimizing overall performance. Although both centralized and distributed [2] algorithms have been widely studied, they often overlook the involvement of human agents (cf. Fig. 1), which is common in applications like manufacturing, disaster response, logistics [3], [4], etc. The presence of humans introduces two key challenges: (i) human preference is dynamic and is influenced by that of nearby autonomous agents, and (ii) human behaviors are inherently uncertain, leading to probabilistic global resource constraints. Our goal is to develop a closed-loop framework with fully distributed algorithm design that enables autonomous robots to anticipate human behavioral responses, incorporate human uncertainty, and collaboratively satisfy globally coupled probabilistic resource constraints, while ensuring efficient resource allocation.

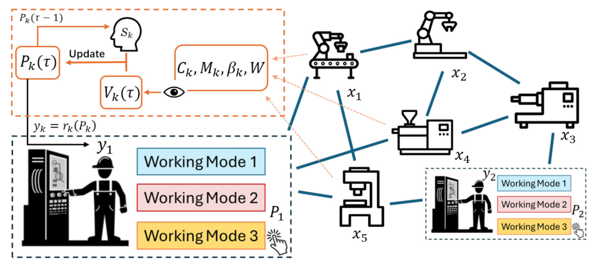

Fig. 1. Resources allocation with humans. Humans choose working modes for themselves, modeled by DFT with uncertainties. $m = 3$, $h = 2$, $\ell_k = 3$.

Literature Review: Advancements in distributed optimization have introduced various methods for resource allocation problems with globally coupled constraints. These include Tracking-ADMM [5], IPLUX [6], and other primal-dual methods [7], [8]. However, these methods are developed under deterministic settings and are not directly applicable to human-involved systems with human response uncertainties.

To model human responses and quantify the uncertainties, insights can be drawn from behavioral economics and psychology, which suggests that human decision-making patterns [9], [10] are impacted by cognitive bias and risk attitudes (risk-seeking vs. risk-averse). This has led to the development of expected utility theory (SEU), prospect theory, regret theory, and decision field theory (DFT) [11], under different engineering contexts [12]. DFT is an important step forward in understanding human decision-making, combining ideas from psychology and behavioral economics. Unlike traditional models that assume fixed preferences and static utility models [13], this theory accounts for how choices change over time and provides a more realistic and dynamic view of human decision-making [11]. The most recent study extends DFT to transportation-related choice problems [10]. However, there is limited literature applying DFT to human-robot collaboration. In this study, we aim to enhance robot's collaboration with humans in a dynamic setting and allow each human-robot pair to complement one another by offsetting mutual limitations while meeting production demands. As

Received 21 May 2025; revised 6 August 2025; accepted 19 August 2025. Date of publication 1 September 2025; date of current version 6 October 2025. This work was supported in part by ARO under Grant W911NF-22-2-0242, and in part by NSF through a LSAMP Bridge to Doctorate fellowship for R. Mbagna Nanko under Grant EPCN 2332210 and Grant EES 2005030. Recommended by Senior Editor Y. Cao.
(Corresponding author: Xuan Wang.)

Yichen Yao and Xuan Wang are with the ECE Department, George Mason University, Fairfax, VA 22101 USA (e-mail: xwang64@gmu.edu).

Ryan Mbagna Nanko and Yue Wang are with the Mechanical Engineering Department, Clemson University, Olney, SC 29634 USA.
Digital Object Identifier 10.1109/LCSYS.2025.3604959

we explore multi-human-multi-robot teaming problems, it is essential to address multi-alternative decision-making for diverse sets of needs [14]. However, existing works do not provide a closed-form solution, which is incompatible with most engineering and machine learning algorithms [15].

Furthermore, while existing works on real-time human-autonomy teaming (HAT) [16], [17], such as resource allocation problems, contribute valuable insights into modeling human uncertainty, they do not account for collective uncertainties introduced by multiple humans, which give rise to globally coupled chance constraints in large-scale multi-agent systems. To address such constraints, sampling-based methods [18] can provide feasible solutions, but they often neglect underlying model structures and suffer from poor scalability as dimensionality increases. Chebyshev inequalities [19] provide distribution-free conservative approximations. However, they require large safety margins and often require centralized computation. Boole's inequality [19] allows decentralization by decomposing the joint constraint into individual ones, but it usually overestimates risk, particularly when constraints are correlated. Other methods to represent the feasible region of the probabilistic constraint include mixed-integer programming [20] or second-order conic [21]. However, these representations are difficult to directly implement in distributed settings, which is critical for achieving scalable deployments in large-scale systems.

Contribution: Focusing on the above-mentioned gaps, this letter incorporates DFT and distributed optimization to address human-autonomy resource allocation. Specifically, we use DFT to model dynamic human preferences influenced by nearby autonomous agents, enabling the prediction of human responses and the quantification of associated uncertainties. Building on this, we exploit the constraint structure to propose a polyhedral approximation of the feasible region for the globally coupled probabilistic constraint represented as linear inequalities. Furthermore, we reformulate the constraint into a locally decoupled form over the communication graph, which allows the design of a decentralized saddle-point algorithm to solve the problem efficiently. The proposed approach is validated by theoretical analysis, discussion on conservativeness, and experiments with human-subject tests.

II. Problem Formulation and Running Example

Consider a system composed of a set of autonomous agents $\mathcal{M} = \{i_1, \dots, i_m\}$, $|\mathcal{M}| = m$ and a set of human agents $\mathcal{H} = \{k_1, \dots, k_h\}$, $|\mathcal{H}| = h$. The agent interactions are represented by an undirected, connected graph $\mathbb{G}$. The vertex set is $\mathcal{V}(\mathbb{G}) = \mathcal{M} \bigcup \mathcal{H}$. The edge set $\mathcal{E}(\mathbb{G})$ defines the neighboring relations: connected agents can observe each other's states and interact. Let $\mathcal{N}_i$, $i \in \mathcal{M}$ and $\mathcal{N}_k$, $k \in \mathcal{H}$ denote the neighbor sets of autonomous agents and humans, respectively. Autonomous agent i controls a state $x_i \in \mathbb{R}^{n_i}$ and a cost function $f_i(\cdot) : \mathbb{R}^{n_i} \to \mathbb{R}$. Human agent k holds a state $y_k \in \mathbb{R}^{s_k}$ and a cost function $g_k(\cdot) : \mathbb{R}^{s_k} \to \mathbb{R}$.

Following multi-alternative DFT [14], we model human preferences over multiple alternatives/options in decision-making using a time-evolving internal state vector $\boldsymbol{P}_k \in \mathbb{R}^{l_k}$ with l_k being the number of alternatives in the choice set. It captures both historical preferences of humans and the influence of neighboring autonomous agents, and evolves:

$$\boldsymbol{P}_k(\tau) = \psi_k\big(x_{\mathcal{N}_k}(\tau), \boldsymbol{P}_k(\tau - 1)\big), \tag{1}$$

where $\psi_k(\cdot)$ is a cognitive update function. Human response $y_k(\tau)$ is then generated as:

$$y_k(\tau) = r_k(\boldsymbol{P}_k(\tau)), \tag{2}$$

where $r_k(\cdot)$ maps internal preferences to observable actions. Due to the stochastic nature of $\boldsymbol{P}_k(\tau)$, the resulting human behavior $y_k(\tau)$ is uncertain and is treated as a random variable with an associated distribution. Further details on the preference update, behavioral generation, and uncertainty modeling will be presented in section.

This behavioral uncertainty affects both the overall system cost and the feasibility of shared resource constraints. Given the prior preference state $\boldsymbol{P}_k(\tau - 1)$, we aim to solve the following optimization problem:

$$\min \mathcal{J}_\tau = \sum_{i\in\mathcal{M}} f_i(x_i(\tau)) + \mathbb{E}\left[\sum_{k\in\mathcal{H}} g_k(y_k(\tau))\right], \tag{3a}$$

subject to the human preference dynamics (1) and response (2), and a global probabilistic resource constraint:

$$\mathbb{P}\left(\sum_{i\in\mathcal{M}} A_i x_i(\tau) + \sum_{k\in\mathcal{H}} B_k y_k(\tau) + c \le 0\right) \ge \delta, \tag{3b}$$

which ensures the resource constraint is satisfied with a confidence level of at least δ.

Example: To illustrate the problem setup, consider in Fig. 1, a smart manufacturing system comprising both robotic and human-operated workstations. The variable x_i denotes the production state of robot i, where each entry represents the production rate of a specific product type. Humans have internal preference states $\boldsymbol{P}_k$ over different working modes, which then map to y_k, denoting the productivity state of human operator k. The preference state depends on surrounding robots' behaviors, updated via the DFT model.

Since human actions are influenced by subjective internal states and are not directly controllable, solving this problem requires autonomous robots to anticipate human behaviors (1)-(2), cooperatively satisfy coupled probabilistic constraints (3b), and minimize the cost (3a).

III. Main Result

Our main results include human preference dynamics modeling, treatment of globally coupled probabilistic resource constraints, and fully distributed algorithm design.

A. Dynamic Human Preference Model

We utilize the DFT to model human k's preference, which evolves dynamically over a discrete time domain τ:

$$\boldsymbol{P}_k(\tau) = \boldsymbol{S}_k \boldsymbol{P}_k(\tau - 1) + \boldsymbol{V}_k(\tau), \tag{4}$$

where the feedback matrix $\boldsymbol{S}_k \in \mathbb{R}^{\ell_k \times \ell_k}$ defines the evolution of preference over time: $\boldsymbol{S}_k = \boldsymbol{I} - \phi_{k,2} \exp(-\phi_{k,1} \boldsymbol{D}_k^2)$, with $\boldsymbol{I} \in \mathbb{R}^{\ell_k \times \ell_k}$ being an identity matrix, scalars $\phi_{k,1}$ representing the human sensitivity to difference in attributes; $\phi_{k,2}$ reflecting the growth/decay rate for past preference. $\boldsymbol{D}_k \in \mathbb{R}^{\ell_k \times \ell_k}$ contains the Euclidean distances between alternatives i, j, for all attributes [10]. $\boldsymbol{V}_k(\tau) \in \mathbb{R}^{\ell_k}$ is a valence vector, representing the choice attributes evaluated by the decision-maker, which can be calculated as [10]:

$$\boldsymbol{V}_k(\tau) = \boldsymbol{C}_k \boldsymbol{M}_k \boldsymbol{\beta}_k \boldsymbol{W}\big(x_{\mathcal{N}_k}(\tau)\big) + \boldsymbol{\varepsilon}_k(\tau) \tag{5}$$

where $\boldsymbol{C}_k \in \mathbb{R}^{\ell_k \times \ell_k}$ is a contrast matrix with elements $c_k^{i,i} = 1$ and $c_k^{i,j\neq i} = -1/(l_k - 1)$, $i, j = 1, \dots, l_k$. It is used to compare between the options for each attribute, allowing for relative evaluation [14]. $\boldsymbol{M}_k \in \mathbb{R}^{\ell_k \times \eta_k}$ is humans' evaluation of the system's η_k attribute values for all the ℓ_k alternatives. Each element is then rescaled by a corresponding attribute scaling coefficient, contained in the diagonal matrix $\boldsymbol{\beta}_k \in \mathbb{R}^{\eta_k \times \eta_k}$. $\boldsymbol{W}(x_{\mathcal{N}_k}(\tau)) \in \mathbb{R}^{\eta_k}$ is a column vector modeling the decision-maker's momentary focus on the attributes. At each time step k, the decision maker's attention focuses on one attribute with probability w_j, where $\sum_{j=1}^{\eta_k} w_j = 1$. Such momentary focus is dependent on the neighboring robot's behavior that the human can observe. The attention weights $\boldsymbol{W}(x_{\mathcal{N}_k}(\tau))$ can be manually prescribed or computed according to an objective criterion. In our implementation, $\boldsymbol{W}$ is computed as a soft-max function of choice attributes. $\boldsymbol{\varepsilon}_k(\tau) \in \mathbb{R}^{\ell_k} \sim \mathcal{N}(0, \sigma_k^2 \boldsymbol{I})$ captures an uncertainty component in the human response as a normal distribution. Putting together (4)-(5) yields human preference dynamics (1). The observable human response $y_k(\tau)$ at time τ is determined by response function (2).

Direct optimization of $\mathcal{J}_\tau$ in (3) is challenging due to the stochasticity of $y_k(\tau)$. To simplify, stochastic processes are approximated using Gaussian distributions and linearization:

$$y_k(\tau) \approx r_k(\boldsymbol{P}_k(\tau-1)) + \nabla r_k(\boldsymbol{P}_k(\tau-1))^\top (\boldsymbol{P}_k(\tau)) - \boldsymbol{P}_k(\tau-1)). \tag{6}$$

We linearize the function at $\boldsymbol{P}_k(\tau-1)$ instead of $\boldsymbol{P}_k(\tau)$ because $\boldsymbol{P}_k(\tau)$ depends on $x_i(\tau)$ which is not known and needs to be designed. This first-order approximation holds under standard regularity assumptions: the function $r_k(\cdot)$ is differentiable and locally Lipschitz around $\boldsymbol{P}_k(\tau-1)$, and the terms $\boldsymbol{P}_k(\tau) - \boldsymbol{P}_k(\tau-1)$, $\sigma_k^2 \boldsymbol{I}$ are sufficiently small.

Combining (4)-(6), it follows that:

$$\mathbb{E}\big[y_k(\tau)\big] \approx H_k\big(x_{\mathcal{N}_k}\big) = \nabla r_k(\boldsymbol{P}_k(\tau-1))^\top \Big((\boldsymbol{S}_k - I)\boldsymbol{P}_k(\tau-1) + \boldsymbol{C}_k \boldsymbol{M}_k \boldsymbol{\beta}_k \mathbb{E}\big[\boldsymbol{W}\big(x_{\mathcal{N}_k}(\tau)\big)\big]\Big) + r_k(\boldsymbol{P}_k(\tau-1)) \tag{7a}$$

$$\Sigma_{y_k(\tau)} \approx \sigma_k^2 \nabla r_k(\boldsymbol{P}_k(\tau-1))^\top \nabla r_k(\boldsymbol{P}_k(\tau-1)). \tag{7b}$$

B. Decoupling the Global Probabilistic Constraint

The above human uncertainty model allows us to analyze the human-autonomy resource allocation in a closed-loop form. In Problem (3), the expectation $\mathbb{E}[g_k(y_k)]$ is generally difficult to evaluate due to the potential nonlinearity of $g_k(\cdot)$ and the uncertainty in y_k. In the following, we adopt a first-order approximation $g_k(\mathbb{E}[y_k]) \approx \mathbb{E}[g_k(y_k)]$. Additionally, since the formulation focuses on a single time step, we omit the time index τ. We rewrite (3) into a compact form.

$$\min_{\mathbf{x}} \quad F(\mathbf{x}) + G\big(\mathbb{E}[\mathbf{y}]\big) \tag{8a}$$

$$\text{s.t.} \quad \mathbb{P}(\mathbf{A}\mathbf{x} + \mathbf{B}\mathbf{y} + c \leq 0) \geq \delta, \tag{8b}$$

$$\mathbf{y} \sim \mathcal{N}\big(\mathbb{E}[\mathbf{y}], \boldsymbol{\Sigma}_{\mathbf{y}}\big), \ \ \mathbb{E}[\mathbf{y}] = \mathbf{H}(\mathbf{x}) \tag{8c}$$

where

$$F(\mathbf{x}) = \sum_{i \in \mathcal{M}} f_i(x_i), \quad G\big(\mathbb{E}[\mathbf{y}]\big) = \sum_{k \in \mathcal{H}} g_k\big(\mathbb{E}[y_k]\big).$$

Here, $\mathbf{x} = \mathrm{col}\{x_{i_1}, \ldots, x_{i_m}\}$ and $\mathbf{y} = \mathrm{col}\{y_{k_1}, \ldots, y_{k_h}\}$ are compact vectors representing the collective states of robotic and human agents. $\mathbf{A} = \big[A_{i_1} \cdots A_{i_m}\big]$, $\mathbf{B} = \big[B_{k_1} \cdots B_{k_h}\big]$ are compact matrices. The distribution of $\mathbf{y}$ is a multivariate Gaussian with mean $\mathbb{E}[\mathbf{y}]$ and covariance $\Sigma_{\mathbf{y}}$, both obtained by aggregating the human preference model in (7). Here, $\mathbf{H}(\mathbf{x}) = \mathrm{col}\{H_{k_1}(x_{\mathcal{N}_{k_1}}), \ldots, H_{k_h}(x_{\mathcal{N}_{k_h}})\}$, where $H_k(\cdot)$ represents the function in (7a); $\boldsymbol{\Sigma}_{\mathbf{y}} = \mathrm{diag}\{\Sigma_{y_{k_1}}, \ldots, \Sigma_{y_{k_h}}\}$. Constraint (8b) is the compact form of (3b).

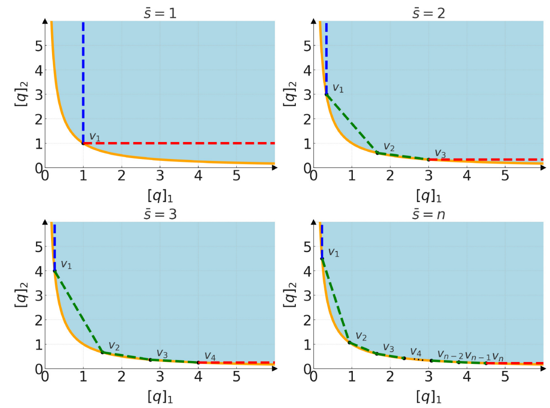

Fig. 2. Visualization of Lemma 1 for $r = 2$. The blue area represents $\mathcal{Q}$. Vertices are associated with (10). Dashed lines are facets of the polyhedron.

The coupled probabilistic constraint (8b) is difficult to handle in a distributed fashion due to its global sum form. In the following, we conservatively approximate this constraint by a deterministic and locally decoupled form over the communication graph. We first present a useful lemma.

Lemma 1 (Polyhedral Approximation of a Probabilistic Feasible Set): The following statements hold.

1) Let $\widehat{\boldsymbol{\zeta}} \sim \mathcal{N}(0, I_r)$ be a standard multivariate normal random vector in $\mathbb{R}^r$, and let $q \in \mathbb{R}^r$. Define the set:
$$\mathcal{Q} = \{q : \mathbb{P}(\widehat{\boldsymbol{\zeta}} \leq q) \geq \delta\}.$$
Then $\mathcal{Q}$ is a closed and convex set.

2) Suppose we construct $\bar{s}$ sets of parameters $\Delta_s = \{\delta_{i,s}\}$ such that $\forall s \in \{1, \ldots, \bar{s}\}$ and $i \in \{1, \ldots, r\}$, the following conditions hold:
$$\delta < \delta_{i,s} < 1, \quad \text{and} \quad \prod_{i=1}^{r} \big(\delta_{i,s}\big) = \delta. \tag{9}$$
Then $\mathcal{Q}$ can be inner approximated by an unbounded polyhedron, defined by $\bar{s} + r + 1$ vertices $\{v \in \mathbb{R}^r\}$:
$$v_s \triangleq \Big[\Phi^{-1}\big(\delta_{1,s}\big), \ldots, \Phi^{-1}\big(\delta_{r,s}\big)\Big]^\top \tag{10a}$$
$$v_{\bar{s}+j} \triangleq \Bigg[+\infty, \ldots, \underbrace{\min_s \Phi^{-1}\big(\delta_{j,s}\big)}_{j\text{-th entry}}, \ldots, +\infty \Bigg]^\top, \tag{10b}$$
$$v_{\bar{s}+r+1} \triangleq [+\infty, \ldots, +\infty]^\top. \tag{10c}$$
where in (10a), $s \in \{1, \ldots, \bar{s}\}$; in (10b), $j \in \{1, \ldots, r\}$, and $\Phi^{-1}(\cdot)$ is the inverse cumulative distribution function (CDF) of the standard normal distribution.
Furthermore, the resulting polyhedron can be equivalently described by an affine inequality $Uq \leq u$, where U is a matrix and u is a vector of proper dimensions. Each row of the inequality corresponds to a facet (bounding hyperplane) of the polyhedron.

We visualize the lemma, in Fig. 2 for $r = 2$ (i.e., 2D case).

Proof of Statement a. Since the components $[\widehat{\boldsymbol{\zeta}}]_i$ are independent standard normal variables, the joint CDF factorizes: $\mathbb{P}(\widehat{\boldsymbol{\zeta}} \leq q) = \prod_{i=1}^{r} \mathbb{P}([\widehat{\boldsymbol{\zeta}}]_i \leq [q]_i) = \prod_{i=1}^{r} \Phi([q]_i)$, where $\Phi(\cdot)$

is the standard normal CDF. It follows that $\log(\mathbb{P}(\widehat{\boldsymbol{\zeta}} \leq q)) = \sum_{i=1}^{r} \log(\Phi([q]_i))$. Since $\Phi(q_i)$ is log-concave, $\mathbb{P}(\widehat{\boldsymbol{\zeta}} \leq q)$ is also log-concave. Therefore, its superlevel set $\mathcal{Q} = \{q:\mathbb{P}(\widehat{\boldsymbol{\zeta}} \leq q) \geq \delta\}$ is convex. The set is closed because the inequality is non-strict.

Proof of Statement b. To construct a polyhedral inner approximation of the convex set $\mathcal{Q}$, we can easily verify that all vertices defined in (10a)–(10c) lie in closed convex set $\mathcal{Q}$. Thus, the convex hull of these vertices forms an inner approximation of $\mathcal{Q}$ as an unbounded polyhedron.

Based on this, inequality $Uq \leq u$ is a direct conclusion of the Minkowski-Weyl theorem [22]: any convex polyhedron can be equivalently represented as the solution set of a finite number of linear inequalities. ■

Before presenting the main result, we define a matrix:

$$\bar{\boldsymbol{\Sigma}} = \sum_{k=1}^{h} B_k \Sigma_{y_k} B_k^\top, \tag{11}$$

which captures the covariance of aggregated human uncertainty over the resource constraint. We make assumptions:

Assumption 1: The following conditions hold.

1) The graph $\mathbb{G}$ is undirected and connected.
2) The matrix $\bar{\boldsymbol{\Sigma}}$ is known to at least one autonomous agent in the system. $\bar{\boldsymbol{\Sigma}}$ has full rank and $\bar{\boldsymbol{\Sigma}}^{1/2} \geq 0$, i.e., its principal square root has all non-negative entries.

Justification: Condition 1) is standard in the literature for distributed optimization [23]. Condition 2) is verifiable and practically feasible. Specifically, the $\bar{\boldsymbol{\Sigma}}$ in (11) only needs a one-time computation, which can be performed using the finite-time averaging (sum) algorithm [24] that adds $B_k \Sigma_{y_k} B_k^\top$ from all agents $k \in \mathcal{H}$. Thus, verifying condition 2) becomes straightforward. The full rank of $\bar{\boldsymbol{\Sigma}}$ is generally true in practice, especially when the dimension of resources r is smaller than that of human states s_k. Moreover, the condition $\bar{\boldsymbol{\Sigma}}^{1/2} \geq 0$ holds for almost all the examples we have tested. This is mainly due to the fact that Σ_{y_k} are positive semi-definite matrices and resource consumption matrices B_k are entry-wise nonnegative (cf. equation (11)). Rigorous conditions on $\bar{\boldsymbol{\Sigma}}^{1/2} \geq 0$ can be found in [25]. •

Theorem 1 (Locally Decouple Sufficient Condition for the Probabilistic Constraint): Consider the following constraint with variables $\mathbf{x}, \mathbf{z}$ and $q \in \mathbb{R}^r$:

$$\text{s.t.} \quad \begin{bmatrix} \bar{\mathbf{A}} & \\ & \bar{\mathbf{B}} \end{bmatrix} \begin{bmatrix} \mathbf{x} \\ \mathbb{E}[\mathbf{y}] \end{bmatrix} + \bar{L}\mathbf{z} + \begin{bmatrix} c + \bar{\boldsymbol{\Sigma}}^{1/2} q \\ \mathbf{0}_{(m+h-1)r} \end{bmatrix} \leq 0 \tag{12a}$$

$$Uq \leq u \tag{12b}$$

where q is a variable associated with a *safe margin* for the probabilistic constraint. $\mathbf{z} = \mathrm{col}\{z_{i_1}, \ldots, z_{i_m}, z_{k_1}, \ldots, z_{k_h}\}$ is a compact variable with components z_i correspond to autonomous agents, and z_k correspond to human agents. $\bar{\mathbf{A}} = \mathrm{diag}\{A_{i_1}, \ldots, A_{i_m}\}$; $\bar{\mathbf{B}} = \mathrm{diag}\{B_{k_1}, \ldots, B_{k_h}\}$; $\bar{L} = L \otimes I_r$ with $L \in \mathbb{R}^{(m+h)\times(m+h)}$ being the Laplacian matrix of graph $\mathbb{G}$. The constraint (12) has the following properties:

1) The reformulated constraint (12a) is equivalent to

$$\big(\mathbf{A}\mathbf{x} + \mathbf{B}\mathbb{E}[\mathbf{y}] + c\big) + \bar{\boldsymbol{\Sigma}}^{1/2} q \leq 0. \tag{13}$$

2) The reformulated constraint (12) is a sufficient condition for the coupled chance constraint (8b).

Proof of Statement a. From the block-diagonal structure of $\bar{\mathbf{A}}$ and $\bar{\mathbf{B}}$, and the compact variables, we observe that:

$$\begin{aligned} &\left(\mathbf{1}_{m+h}^\top \otimes I_r\right)\left(\begin{bmatrix} \bar{\mathbf{A}} & \\ & \bar{\mathbf{B}} \end{bmatrix}\begin{bmatrix} \mathbf{x} \\ \mathbb{E}[\mathbf{y}] \end{bmatrix} + \begin{bmatrix} c + \bar{\boldsymbol{\Sigma}}^{1/2} q \\ \mathbf{0} \end{bmatrix}\right) \\ &\qquad = \mathbf{A}\mathbf{x} + \mathbf{B}\mathbb{E}[\mathbf{y}] + c + \bar{\boldsymbol{\Sigma}}^{1/2} q. \end{aligned} \tag{14}$$

Since $\mathbb{G}$ is connected and undirected, $\ker(L) = \ker(L^\top)$ is the column span of $\mathbf{1}_{m+h}$. It follows that $\ker(\mathbf{1}_{m+h}^\top) = \mathrm{image}(L)$. Using Kronecker product, one has $\ker(\mathbf{1}_{m+h}^\top \otimes I_r) = \mathrm{image}(\bar{L})$ and $(\mathbf{1}_{m+h}^\top \otimes I_r)\bar{L} = 0$. Based on this and (14), multiplying $(\mathbf{1}_{m+h}^\top \otimes I_r)$ on (12a) yields (13).

Now, we show (13) yields (12a). By (13) and (14), there must exist a vector $\xi \geq 0$, such that

$$\left(\mathbf{1}_{m+h}^\top \otimes I_r\right)\left(\begin{bmatrix} \bar{\mathbf{A}} & \\ & \bar{\mathbf{B}} \end{bmatrix}\begin{bmatrix} \mathbf{x} \\ \mathbb{E}[\mathbf{y}] \end{bmatrix} + \begin{bmatrix} c + \bar{\boldsymbol{\Sigma}}^{1/2} q \\ 0 \end{bmatrix} + \xi\right) = 0,$$

Consequently, since $\ker(\mathbf{1}_{m+h}^\top \otimes I_r) = \mathrm{image}(\bar{L})$, there always exists a $\mathbf{z}$ such that

$$\begin{bmatrix} \bar{\mathbf{A}} & \\ & \bar{\mathbf{B}} \end{bmatrix}\begin{bmatrix} \mathbf{x} \\ \mathbb{E}[\mathbf{y}] \end{bmatrix} + \begin{bmatrix} c + \bar{\boldsymbol{\Sigma}}^{1/2} q \\ 0 \end{bmatrix} + \xi = -\bar{L}\mathbf{z} \tag{15}$$

Since $\xi \geq 0$, one has (12a) is true.

Proof of Statement b. We show that (12) implies $\mathbb{P}(\mathbf{A}\mathbf{x} + \mathbf{B}\mathbf{y} + \mathbf{c} \leq 0) \geq \delta$. First, note that

$$\begin{aligned} &\mathbb{P}(\mathbf{A}\mathbf{x} + \mathbf{B}\mathbf{y} + c \leq 0) \\ &\quad = \mathbb{P}\big(\mathbf{B}(\mathbf{y} - \mathbb{E}[\mathbf{y}]) \leq -(\mathbf{A}\mathbf{x} + \mathbf{B}\mathbb{E}[\mathbf{y}] + c)\big) \\ &\quad \geq \mathbb{P}\Big(\mathbf{B}(\mathbf{y} - \mathbb{E}[\mathbf{y}]) \leq \bar{\boldsymbol{\Sigma}}^{1/2} q\Big), \end{aligned} \tag{16}$$

where the inequality follows from (13).

To continue, note that multiplication of entry-wise non-negative matrices preserves vector inequalities, thus, one has

$$\mathbb{P}\Big(\mathbf{B}(\mathbf{y} - \mathbb{E}[\mathbf{y}]) \leq \bar{\boldsymbol{\Sigma}}^{1/2} q\Big) \geq \mathbb{P}\Big(\bar{\boldsymbol{\Sigma}}^{-1/2}\mathbf{B}(\mathbf{y} - \mathbb{E}[\mathbf{y}]) \leq q\Big), \tag{17}$$

where the condition on the right is sufficient for that on the left by multiplying $\bar{\boldsymbol{\Sigma}}^{1/2}$, which is entry-wise non-negative due to Assumption 1.

Next, define the standardized variable

$$\widehat{\boldsymbol{\zeta}} = \bar{\boldsymbol{\Sigma}}^{-1/2}\mathbf{B}\big(\mathbf{y} - \mathbb{E}[\mathbf{y}]\big) \sim \mathcal{N}(0, I_r). \tag{18}$$

Combining (16), (17), and (18), one has:

$$\mathbb{P}(\mathbf{A}\mathbf{x} + \mathbf{B}\mathbf{y} + c \leq 0) \geq \mathbb{P}\big(\widehat{\boldsymbol{\zeta}} \leq q\big) \leq \delta.$$

where the last inequality holds because $Uq \leq u$ implies $q \in \mathcal{Q}$ by Lemma 1(b). ■

Remark 1 (Conservativeness): Reformulation (12) is a conservative approximation of the probabilistic constraint (8b), where $\bar{\boldsymbol{\Sigma}}^{1/2} q$ is an extra *safe margin* to ensure the constraint is not violated. The conservativeness arises from two sources: (i) The inner approximation of $\mathcal{Q}$ using a polyhedral set. As illustrated in Fig. 2, this conservativeness can be reduced by increasing the number of approximation points. (ii) The use of $\bar{\boldsymbol{\Sigma}}^{1/2}$ to establish a sufficient condition in (17). This condition is sufficient, it is not necessary unless $\bar{\boldsymbol{\Sigma}}^{-1/2} \geq 0$, which is generally hard to ensure. Nevertheless, since $\bar{\boldsymbol{\Sigma}}^{1/2}$ depends on the covariance of the human response $\mathbf{y}$, the resulting conservativeness diminishes when the uncertainty in human response is low. •

Constraint (12) is fully distributed, i.e., each agent only requires local information from its neighbors to verify feasibility (each row of (12)). If using the Lagrangian method and saddle point dynamics to solve the problem, this structure naturally leads to the following distributed algorithm.

C. Distributed Saddle-Point Dynamics

Define augmented Lagrangian function:

$$\mathcal{L}(\mathbf{x}, \mathbf{z}, q, \boldsymbol{\lambda}, \mu) = F(\mathbf{x}) + G(\mathbf{H}(\mathbf{x})) + \mu^\top (Uq - u) \\ +\boldsymbol{\lambda}^\top \left(\begin{bmatrix} \bar{\mathbf{A}} & \\ & \bar{\mathbf{B}} \end{bmatrix} \begin{bmatrix} \mathbf{x} \\ \mathbf{H}(\mathbf{x}) \end{bmatrix} + \bar{L}\mathbf{z} + \begin{bmatrix} c + \bar{\boldsymbol{\Sigma}}^{1/2} q \\ \mathbf{0}_{(m+h-1)r} \end{bmatrix} \right) \quad (19)$$

where $\boldsymbol{\lambda} \in \mathbb{R}^{(m+h)r}$ and $\boldsymbol{\mu} \in \mathbb{R}^d$ are the dual variables associated with constraints (12a) and (12b), respectively. Also, based on (8c), we replaced $\mathbb{E}[\mathbf{y}]$ with $\mathbf{H}(\mathbf{x})$.

Corollary 1: The saddle-point dynamics that achieve equilibrium of (19) yield a fully distributed algorithm for solving (8) with reformulated constraint (12).

We simply show agent-wise dynamics to validate Corollary 1. By exploiting the structure of the Laplace matrix $\bar{L}$, state dependencies among agents only happen among neighbors. The dynamics for autonomous agent $i \in \mathcal{M}$:

$$\dot{x}_i = -\nabla f_i(x_i) - \sum_{k \in (\mathcal{N}_i \bigcup \mathcal{H})} \left(H_{i,k}^\top \left(\nabla g_k(\mathbb{E}[y_k] + B_k^\top \lambda_k) \right) \right) - A_i^\top \lambda_i$$

$$\dot{z}_i = -\sum_{j \in \mathcal{N}_i} (\lambda_i - \lambda_j)$$

$$\dot{\lambda}_i = \begin{cases} \left[A_i x_i + \sum_{j \in \mathcal{N}_i} (z_i - z_j) + c_i + \bar{\boldsymbol{\Sigma}}^{1/2} q \right]_+, & i = i_1 \\ \left[A_i x_i + \sum_{j \in \mathcal{N}_i} (z_i - z_j) \right]_+. & \text{others} \end{cases}$$

where $H_{i,k} \triangleq \frac{\partial H_k(x_{\mathcal{N}_k})}{\partial x_i}$ with $H_k(\cdot)$ in (7a), $[\,\cdot\,]_+$ projects any negative entries of a vector to zero. Additionally, agent i_1 (or any other agent) also updates *safe margin* variables:

$$\dot{q} = -\bar{\boldsymbol{\Sigma}}^{1/2^\top} \lambda_1 - U^\top \mu, \quad \text{and} \quad \dot{\mu} = [Uq - u]_+,$$

The dynamics for human agent $k \in \mathcal{H}$:

$$\dot{z}_k = -\sum_{j \in \mathcal{N}_k} (z_k - z_j), \quad \text{and} \quad \dot{\lambda}_k = \left[B_k \mathbb{E}[y_k] + z_k \right]_+.$$

Here, the expected human response $\mathbb{E}[y_k]$ does not follow an algorithmic update, but is predicted using the model (7a).

Remark 2: The main focus of this letter is the reformulation of the coupled probabilistic constraint into a fully decoupled and distributed form, as presented in Theorem 1. This reformulation enables the design of fully distributed saddle point dynamics, under which the states of all agents asymptotically converge to the optimal solution of Problem (3). The convergence proof is omitted, as it follows directly from standard analyses of saddle point dynamics [26]. •

IV. EXPERIMENTS WITH HUMAN SUBJECT TESTS

We present simulated experiments with real human subject tests to evaluate the performance of the proposed method in terms of constraint satisfaction and system cost. The experimental procedure meets Clemson University's Institutional Review Board guidelines for expedited review under 45 CFR 46.110 and 46.111. IRB Number: IRB2025-0013. The design of our experiments draws upon prior works in decision field theory, human choice modeling [27], and uncertainty-aware optimization [12], [18], [20]. Due to space limits, we only present experiment results. Details of experiments and human-subject tests are provided on the project Website: https://github.com/GMU-MICO/Distributed-Human-Autonomy.

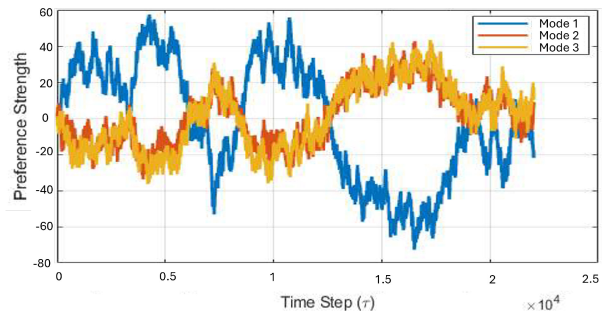

Fig. 3. Human preference evolution ($\phi_{k,1} = 18.9135$, $\phi_{k,2} = 0.1858$, $\boldsymbol{\varepsilon}_k = 1$). **DFT Results:** $\mathbb{E}[\boldsymbol{P}_k] = [2.25, -0.62, -1.69]$. Choice probabilities: $[0.929, 0.053, 0.018]$.

1) System Setup: As shown in Fig. 1, we consider a production system consisting of five autonomous agents and two human workers. We let $x_i \in \mathbb{R}^3$, $y_k \in \mathbb{R}^4$, which means autonomous agents and humans may produce three and four types of products, respectively. Let $A_i \in \mathbb{R}^{3\times 3}$ and $B_k \in \mathbb{R}^{4\times 3}$, which maps production to three types of resources, i.e., $c \in \mathbb{R}^3$. The cost functions $f_i(x_i)$, $g_k(y_k)$ follow quadratic forms.

2) Human Subject Test: We conducted a human-subject experiment with 8 participants, each session lasting about an hour, where a custom GUI (Graphical User-Interface) was used to assess user preferences. Each session consisted of 40 trials per participant, resulting in 320 total trials across eight participants. Among the collected 320 choice observations, 240 data points were used to learn preference dynamics, and the remaining 80 were reserved for validation. The internal preference state $\boldsymbol{P}_k \in \mathbb{R}^3$ characterizes each human worker's subjective evaluation over three available working-mode options. These modes are described by five key attributes: energy consumption, safety, intelligence, reliability, and pace. Participants' responses are collected under different task scenarios (e.g., high vs. low urgency). By varying these variables, we make up the attribute matrix $\boldsymbol{M}_k$ and observe the user choice probability. For each trial, the user's attention toward a given choice problem is modeled by the vector $\boldsymbol{W}(x_{\mathcal{N}_k}(\tau))$. This is a weighting vector that sums to 1, representing the allocation of attention. The attention weights are computed as a softmax function of choice attributes, which are influenced by the behaviors of the neighboring autonomous agents $x_{\mathcal{N}_k}(\tau)$.

The GUI allows human-centric pairing predictions. Other DFT parameters ($\phi_{k,1}, \phi_{k,2}, \boldsymbol{\varepsilon}_k, \boldsymbol{\beta}_k$) are estimated via Apollo choice modeling software [27]. These parameters are then used to predict user choices, which participants confirm accuracy within the GUI. An example of human preference dynamics with identified parameters is given in Fig. 3. The prediction accuracy of the models reaches a peak of 79.3% among all eight participants.

3) Algorithm Validation and Conservativeness: We evaluate the proposed algorithm under different probabilistic confidence levels, $\delta \in \{0.6, 0.7, 0.8, 0.9\}$. For each δ, we solve the human-involved resource allocation problem by testing 1000 samples of y_k from the modeled distribution. To measure the system performance under human uncertainty, we additionally consider a constraint violation penalty:

$$\text{Penalty} = \left\| \text{maxv} \left(0, \sum_i A_i x_i + \sum_k B_k y_k + c \right) \right\|_2,$$

TABLE I
PROBABILISTIC CONSTRAINT SATISFACTION **RATE** AND **PENALTY**, SYSTEM OBJECTIVE FUNCTION **COST**, AND **PERFORMANCE** INDEX UNDER DIFFERENT SETTINGS. ↑ MEANS LARGER IS BETTER, AND VICE VERSA

Metric	$\delta = 0.6$	$\delta = 0.7$	$\delta = 0.8$	$\delta = 0.9$	BL1	BL2
Rate ↑	81.3%	88.7%	91.2%	94.1%	43.6%	27.4%
Penalty ↓	23.6	13.7	8.2	6.9	123.8	180.7
Cost ↓	24.6	26.1	28.6	29.3	22.4	40.1
Performance ↓	48.2	39.8	36.8	35.5	146.2	220.8

where $\mathrm{maxv}(\cdot)$ takes entry-wise max that captures the violation of each resource. The overall performance index is:

$$\text{Performance Index} = \text{Cost} + \gamma \cdot \text{Penalty}, \ \ \gamma = 1$$

Experiment results are summarized in Table I.

We compare our method against two baselines. BL1 uses expected human response ($\mathbb{E}[y_k]$), ignoring uncertainty (Σ_{y_k}). BL2 uses previous human responses $y_k(\tau - 1)$ for the new timestep, ignoring both human response and uncertainty.

From the table, the constraint satisfaction rate and penalty rows verify the effectiveness of our algorithm for handling human uncertainty. The proposed algorithm can achieve the required confidence level. The satisfaction rate is known to be conservative (cf. Remark 1). The conservativeness drops as δ goes up. BL 1 and 2 both have large violations of constraints, due to not considering human uncertainties. The system cost row verifies the quality of human responses' prediction. All methods significantly outperform BL 2, which highlights the benefit of incorporating predictive models. However, stricter confidence levels δ lead to slightly higher costs due to increased safety margins that restrict resource flexibility. The overall performance index balances cost and constraint violation. Our method outperforms both baselines across all settings. The tuning of δ can optimize system performance by balancing robustness and efficiency.

V. CONCLUSION AND LIMITATIONS

We proposed a fully distributed optimization framework for human-autonomy resource allocation under globally coupled probabilistic constraints, which could benefit real-world human-autonomy teaming applications, such as collaborative multi-robot systems, and human-in-the-loop logistics planning. Using DFT, we captured human preference dynamics and quantified the associated uncertainty. We reformulated the joint chance constraint into a tractable, locally decoupled form using polyhedral approximation, which enabled a distributed saddle-point algorithm to solve the allocation problem. The proposed method was validated through theoretical analysis and human-subject experiments. The proposed algorithm is fully distributed: each agent's per-iteration cost scales with its number of neighbors, enabling scalability in sparse networks. However, as the system grows and the network becomes more complex, convergence may slow down, increasing overall computation and communication complexity. Besides, the current method does not support mixed-integer constraints, which commonly arise in real-world planning and coordination tasks. Future works will address these limitations, as well as optimize scalability through network structure design.

REFERENCES

[1] M. Doostmohammadian et al., "Survey of distributed algorithms for resource allocation over multi-agent systems," *Annu. Rev. Control*, vol. 59, Jan. 2025, Art. no. 100983.
[2] X. Wang, S. Mou, and B. D. Anderson, "Consensus-based distributed optimization enhanced by integral feedback," *IEEE Trans. Autom. Control*, vol. 68, no. 3, pp. 1894–1901, Mar. 2023.
[3] F. Ranz, V. Hummel, and W. Sihn, "Capability-based task allocation in human-robot collaboration," *Procedia Manuf.*, vol. 9, pp. 182–189, Jan. 2017.
[4] Y. Yao, R. M. Nanko, Y. Wang, and X. Wang, "Distributed resource allocation for human-autonomy teaming under coupled constraints," 2025, *arXiv:2504.02088*.
[5] A. Falsone, I. Notarnicola, G. Notarstefano, and M. Prandini, "Tracking-ADMM for distributed constraint-coupled optimization," *Automatica*, vol. 117, Jul. 2020, Art. no. 108962.
[6] X. Wu, H. Wang, and J. Lu, "Distributed optimization with coupling constraints," *IEEE Trans. Autom. Control*, vol. 68, no. 3, pp. 1847–1854, Mar. 2023.
[7] G. Banjac, F. Rey, P. Goulart, and J. Lygeros, "Decentralized resource allocation via dual consensus ADMM," in *Proc. Amer. Control Conf. (ACC)*, 2019, pp. 2789–2794.
[8] X. Wang and S. Mou, "A distributed algorithm for achieving the conservation principle," in *Proc. Annu. Amer. Control Conf. (ACC)*, 2018, pp. 5863–5867.
[9] D. Kahneman, *Thinking, Fast and Slow*, 1st ed. New York, NY, USA: Farrar, Straus Giroux, 2011.
[10] T. O. Hancock, S. Hess, C. F. Choudhury, and P. Tsoleridis, "Decision field theory: An extension for real-world settings," *J. Choice Model.*, vol. 52, Sep. 2024, Art. no. 100495.
[11] J. R. Busemeyer and J. T. Townsend, "Decision field theory: A dynamic-cognitive approach to decision making in an uncertain environment," *Psychol. Rev.*, vol. 100, no. 3, pp. 432–459, 1993.
[12] L. Jiang, D. Chen, Z. Li, and Y. Wang, "Risk representation, perception, and propensity in an integrated human lane-change decision model," *IEEE Trans. Intell. Transp. Syst.*, vol. 23, no. 12, pp. 23474–23487, Dec. 2022.
[13] V. Köbberling and P. P. Wakker, "Preference foundations for nonexpected utility: A generalized and simplified technique," *Math. Oper. Res.*, vol. 28, no. 3, pp. 395–423, 2003.
[14] R. M. Roe, J. R. Busemeyer, and J. T. Townsend, "Multialternative decision field theory: A dynamic connectionst model of decision making," *Psychol. Rev.*, vol. 108, no. 2, pp. 370–392, 2001.
[15] A. Hämäläinen, M. M. Çelikok, and S. Kaski, "Differentiable user models," in *Proc. 39th Conf. Uncertain. Artif. Intell.*, 2023, pp. 798–808.
[16] D. Fridovich-Keil et al., "Confidence-aware motion prediction for real-time collision avoidance1," *Int. J. Robot. Res.*, vol. 39, nos. 2–3, pp. 250–265, 2020.
[17] S. Nikolaidis, D. Hsu, and S. Srinivasa, "Human-robot mutual adaptation in collaborative tasks: Models and experiments," *Int. J. Robot. Res.*, vol. 36, nos. 5–7, pp. 618–634, 2017.
[18] J. C. Helton, J. D. Johnson, C. J. Sallaberry, and C. B. Storlie, "Survey of sampling-based methods for uncertainty and sensitivity analysis," *Rel. Eng. Syst. Saf.*, vol. 91, nos. 10–11, pp. 1175–1209, 2006.
[19] G. Grimmett and D. Stirzaker, *Probability and Random Processes*. Oxford, U.K.: Oxford Univ. Press, 2020.
[20] S. Küçükyavuz and R. Jiang, "Chance-constrained optimization: A review of mixed-integer conic formulations and applications," 2021, *arXiv:2101.08746*.
[21] C. M. Lagoa, X. Li, and M. Sznaier, "Application of probabilistically constrained linear programs to risk-adjusted controller design," in *Proc. Amer. Control Conf.*, 2001, pp. 738–743.
[22] C. Weibel, "Minkowski sums of polytopes: Combinatorics and computation," Ph.D. dissertation, Faculté Des Sci. De Base, EPFL, Lausanne, Switzerland, 2007.
[23] A. Nedic and A. Ozdaglar, "Distributed subgradient methods for multi-agent optimization," *IEEE Trans. Autom. Control*, vol. 54, no. 1, pp. 48–61, Jan. 2009.
[24] S. Mou and A. S. Morse, "Finite-time distributed averaging," in *Proc. Amer. Control Conf.*, 2014, pp. 5260–5263.
[25] B.-S. Tam and P.-R. Huang, "Nonnegative square roots of matrices," *Linear Algebra Appl.*, vol. 498, pp. 404–440, Jun. 2016.
[26] A. Cherukuri, E. Mallada, and J. Cortés, "Asymptotic convergence of constrained primal–dual dynamics," *Syst. Control Lett.*, vol. 87, pp. 10–15, Jan. 2016.
[27] S. Hess and D. A. Palma, "Apollo: A flexible, powerful and customisable freeware package for choice model estimation and application," *J. Choice Model.*, vol. 32, Sep. 2019, Art. no. 100170.